Journal of Electronics and Electrical Engineering
https://ojs.wiserpub.com/index.php/JEEE

UNIVERSAL WISER PUBLISHER

Review

Review of Sensorless Control Technology for Flywheel Energy Storage PMSM

Shuya Yang[1], Junying Wei[1*], Jihong Wang[2†], Shouqi Liu[1], Yang Yu[1]

[1] School of Energy Storage Technology, Shandong University of Science and Technology, Qingdao, 266590, China
[2] School of Engineering, University of Warwick, Coventry, CV4 7AL, United Kingdom
E-mail: skd992486@sdust.edu.cn, Jihong.Wang@warwick.ac.uk

Received: 29 April 2026; **Revised:** 6 July 2026; **Accepted:** 14 July 2026; **Published:** 20 August 2026

Abstract: Sensorless control of the Permanent Magnet Synchronous Motor (PMSM) is a key technology for achieving high efficiency and reliable operation in Flywheel Energy Storage Systems (FESS). This review focuses on sensorless control techniques suitable for the wide speed range and high dynamic response of FESS, covering methods for zero/low-speed, medium/high-speed, and full-speed operation. First, the fundamentals of sensorless control for FESS motors (mainly PMSM) are analyzed, and the principles and advantages of high-frequency signal injection methods in the zero/low-speed range are compared, along with their limitations in standby and startup scenarios of the flywheel. Second, recent advances in model-based methods-such as sliding mode observers and model reference adaptive systems-for the medium/high-speed range are elaborated. By comparing the strengths and weaknesses of each method under charging, discharging, and standby conditions, targeted improvement strategies are summarized, and a full-speed sensorless control strategy tailored to the FESS PMSM is proposed. Finally, future trends are discussed in the context of practical FESS applications, including online parameter identification, fault-tolerant control, and the integration of intelligent algorithms.

Keywords: flywheel energy storage, Permanent Magnet Synchronous Motor (PMSM), sensorless control, position estimation, wide-speed-range control

1. Introduction

The Flywheel Energy Storage System (FESS) is a physical energy storage technology that stores electrical energy as mechanical energy in a high-speed rotating flywheel. It offers significant advantages, including fast response, long cycle life, high energy conversion efficiency, high power density, deep charge/discharge capability, and environmental friendliness [1]-[3]. In recent years, as the penetration of renewable energy generation continues to increase and the demand for frequency regulation and power support in power grids grows, FESS-as a high-quality solution for short-term, high-power energy storage-has shown broad application prospects in grid frequency regulation, microgrid stabilization, uninterruptible power supplies, electric vehicle energy recovery, and aerospace [2].

Typical FESS components include flywheel rotors, drive motors/generators, bearing systems, power electronic converters, and control systems. Among these components, the control performance of the drive motor directly affects the energy storage efficiency and operational reliability of the system. FESS operates over a wide speed range and involves multiple working conditions, including charging, discharging, and standby. The motor is required to accelerate

DOI: https://doi.org/10.37256/jeee.52202610089

and decelerate frequently during charging and discharging processes, which imposes high demands on the dynamic performance and robustness of the drive control system [3].

In conventional high-performance motor drive systems, rotor position and speed information is typically obtained using mechanical position sensors such as optical encoders and resolvers. However, in industrial applications of large-capacity FESS, speed sensors may become unreliable due to external disturbances, making it difficult to accurately obtain rotor angle and speed information [4]. Issues such as high sensor cost, limited installation space, and reduced reliability under high-speed and high-temperature conditions further constrain the compact design and long-term stable operation of FESS. Therefore, sensorless control technology has become a research focus in the field of flywheel energy storage. Its core concept is to use measurable electrical signals-such as voltage and current-to estimate rotor position and speed online via appropriate estimation algorithms, thereby replacing traditional mechanical sensors.

Sensorless control techniques for FESS motors can be classified into two categories based on estimation principles and applicable speed ranges. The first category is the high-frequency signal injection method, suitable for zero/low-speed ranges. This method exploits the saliency effect caused by the inductance asymmetry between the direct and quadrature axes (d-q axes) of the motor. It injects a high-frequency voltage signal and demodulates the rotor position information from the resulting current response. The second category includes model-based observation methods suitable for medium/high-speed ranges, such as sliding mode observers, model reference adaptive systems, and Kalman filters, which are based on back Electromotive Force (back-EMF) observation [5]. In recent years, with the rapid development of online parameter identification, fault-tolerant control, and intelligent algorithm integration, significant progress has been made in the estimation accuracy, dynamic response, and robustness of sensorless control for FESS [6].

This review presents sensorless control techniques that can be tailored to the wide speed range and high dynamic response characteristics of FESS, with particular attention to methods suitable for zero/low-speed and medium/high-speed operation. First, the operating principle of FESS and the fundamentals of sensorless control are analyzed. Second, the basic principles and research progress of high-frequency signal injection methods for the zero/low-speed range, together with model-based observation methods (such as sliding mode observers, model reference adaptive systems, and Kalman filters) for the medium/high-speed range, are systematically discussed. Finally, a full-speed hybrid control strategy dedicated to FESS is proposed, followed by an outlook on potential future trends in sensorless control technology, including online parameter identification, fault-tolerant control, and the integration of intelligent algorithms.

2. Fundamentals of FESS motors and sensorless control

2.1 *Types and characteristics of mainstream FESS motors*

Special performance requirements are imposed on motors in FESS. On one hand, extremely high rotational speeds-typically tens of thousands to even hundreds of thousands of revolutions per minute-need to be withstood. On the other hand, frequent switching between charging and discharging conditions is required, and extremely low no-load losses are needed to maintain long-term standby operation. Three main types of motors can be considered for FESS: Permanent Magnet Synchronous Motors (PMSM), Switched Reluctance Motors (SRM), and Induction Motors (IM) [7].

(1) PMSM: This type can be divided into Surface-Mounted (SPMSM) and Interior (IPMSM) configurations. PMSM offers advantages such as high power density, high efficiency, high power factor, and a wide speed regulation range. High-precision speed and torque control can be achieved through vector control, making PMSM the preferred motor type for medium-to-high-end FESS. IPMSM is often adopted in high-speed FESS, where the saliency characteristic can be utilized to enhance power density via reluctance torque, and higher mechanical strength can be provided to accommodate high-speed rotation.

(2) SRM: A simple structure, low cost, strong fault tolerance, and adaptability to high-temperature and high-speed environments are exhibited by SRM. However, drawbacks such as high torque ripple, high noise, and complex control are also associated with SRM. It is mainly employed in cost-sensitive, low-to-medium power FESS applications.

(3) IM: Reliable structure and low cost are offered by IM, but power density and efficiency are lower than those of PMSM. Considerable rotor losses may be generated during high-speed operation. IM is therefore used only in traditional low-performance FESS.

Given the significant performance advantages of PMSM, this review focuses on sensorless control techniques for PMSM.

2.2 *Core principle and control framework of sensorless control*

The core principle of sensorless motor control can be stated as follows: using directly measurable electrical parameters (e.g., voltage and current) in conjunction with motor mathematical models or dedicated signal processing methods, rotor position angle and rotational speed may be estimated in real time. Thus, the signals of physical sensors are replaced, and critical feedback information is supplied for advanced control strategies, including vector control and direct torque control.

A typical framework for sensorless control of FESS motors can be divided into three parts. A signal acquisition module is responsible for the collection of signals such as stator voltage, stator current, and DC-link voltage. A position/speed estimation module processes the acquired signals based on specific algorithms, from which estimated rotor position and rotational speed are output. A core control module takes the estimated values as feedback, by which torque/speed control of the motor is realized, thus satisfying the charging and discharging requirements of the flywheel. During charging, the motor operates in motoring mode to drive the flywheel to accelerate; during discharging, it operates in generating mode to convert the kinetic energy of the flywheel into electrical energy.

The accuracy and real-time performance of position/speed estimation are considered to be the key aspects of sensorless control, by which the stability of motor control is directly determined. Under the operating conditions of FESS, such as a wide speed range and high-speed parameter variations, the estimation algorithm is required to address robustness during low-speed startup, accuracy during high-speed operation, and smoothness during dynamic transitions.

3. Control for zero/low-speed operation

When a permanent magnet synchronous motor operates in the zero/low-speed range, the back-EMF amplitude is extremely low, and the signal-to-noise ratio deteriorates significantly. Under such conditions, observer methods based on the fundamental motor model may not be effective in extracting rotor position information [8]. Therefore, sensorless operation is typically achieved using open-loop control methods or high-frequency signal injection methods. Open-loop control methods mainly include Voltage/Frequency (V/F) control and Current/Frequency (I/F) control. These methods are simple in algorithm and easy to implement, but their anti-disturbance capability is limited [9], [10]. The high-frequency signal injection method, on the other hand, injects a high-frequency voltage signal and utilizes the saliency characteristic of the motor for rotor position identification. This method is suitable for applications with high starting performance requirements [11]. In recent years, extensive improvement studies have been carried out to address the shortcomings of the above methods in terms of filter delay, noise suppression, and saliency dependence. Significant progress has been achieved in this area.

3.1 *V/F control*

By maintaining a constant ratio between voltage and frequency, V/F control ensures that the motor flux Φ_m remains unchanged, thereby enabling motor speed regulation. When the back-EMF is sufficiently large, the voltage drop across the stator resistance can be neglected, and the phase voltage is approximately equal to the induced electromotive force. The relationship between these quantities is expressed in Equation (1):

$$E \approx U_s = 4.44\, f\, N_s\, K\, \Phi_m \tag{1}$$

$$\frac{U_s}{f} = 4.44\, N_s\, K\, \Phi_m = \text{constant}. \tag{2}$$

Where f is the stator current frequency, N_s is the number of series turns per phase winding, K is the winding coefficient, Φ_m is the air-gap magnetic flux per pole, E is the back-EMF, and U_s is the phase voltage.

Open-loop V/F control does not rely on motor parameters and has a simple control structure. It can be applied to both surface-mounted and interior permanent magnet synchronous motors. However, the V/F curve is usually determined through offline tests, and problems such as current oscillation, loss of synchronism, or stalling may occur under transient load overshoot conditions. To address these limitations, Reference [12] adopts an improved V/F control strategy with low-frequency voltage compensation. Based on the V/F characteristic curve, an extra voltage compensation unit is introduced. A compensation voltage approximately equal to the voltage drop across the stator resistance is applied to lift the voltage in the low-frequency region, so as to compensate the voltage loss induced by stator resistance and leakage inductance. This strategy enhances the starting performance at zero and low speeds and avoids startup failure. Reference [13] proposes a V/F control strategy with a speed feedback loop for permanent magnet synchronous motors. A PI observer is adopted to estimate the rotor speed and correct the stator voltage in real time, so as to realize high-performance improved V/F control.

3.2 *I/F control*

I/F control maintains current stability through closed-loop current regulation and realizes stable operation by exploiting the torque-load angle self-balancing characteristic of electric machines. This strategy avoids excessive current and simultaneously improves the output torque capability, with its control procedure depicted in Figure 1 [14], and the definitions of variables in the diagram are listed in Table 1. Nevertheless, conventional I/F control suffers from pronounced speed oscillation and weak disturbance rejection during the open-loop starting phase, and a relatively long transition period is needed for switching to closed-loop control in the medium-high speed range. Compared with V/F control, I/F control introduces a closed-loop current regulator, which addresses the problem of uncontrolled current encountered in V/F control.

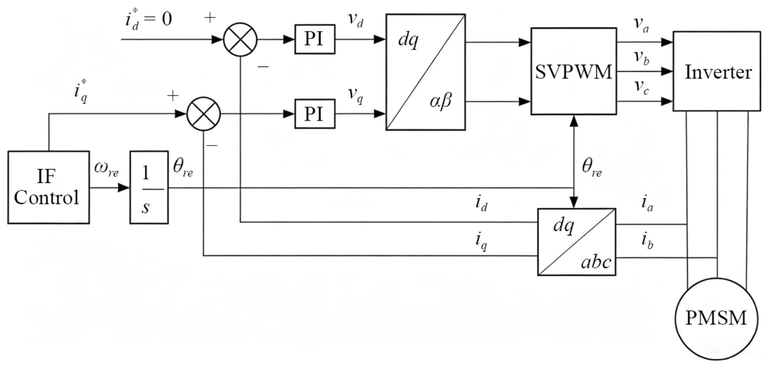

Figure 1. Block diagram of the I/F control process

The basic principle of I/F control is to utilize the torque-load angle self-balancing characteristic of the machine, as given in Equation (3). Closed-loop current regulation is employed to ensure current stability and achieve direct control of the torque-producing current. The rotor position is acquired by integrating the given current frequency, which prevents overcurrent and elevates the output torque capacity [15].

$$T_e \approx 1.5\, p\, i_q^* \sin(\theta_L)\, \psi_f. \tag{3}$$

Where T_e is the electromagnetic torque, p is the number of pole pairs, i_q^* is the q-axis reference current, θ_L is the load angle between the stator current vector and the rotor flux linkage vector, and ψ_f is the permanent magnet flux linkage.

The startup process under I/F control is divided into three sequential stages: pre-positioning, uniform acceleration, and constant-speed operation [16]. When load torque varies, the load angle is automatically adjusted by the system based on the torque-load angle self-balancing characteristic, thereby establishing a new steady-state equilibrium.

I/F control has been adopted for motor startup and speed ramp-up in Reference [17], yielding a simple, stable, and low-cost startup scheme. A compensated I/F startup method is proposed in Reference [18], where a current amplitude compensation loop is utilized to suppress load disturbances once the motor reaches a specified rotational speed, enabling a smooth transition to the medium-high speed region. Nevertheless, I/F control remains essentially an open-loop control strategy. It is characterized by relatively poor stability and a high risk of out-of-step operation, and thus is only applicable to scenarios with low requirements for startup performance.

Table 1. Description of symbols in the I/F control block diagram

Symbol	Description
i_d^*	d-axis current reference (typically zero)
i_q^*	Virtual q-axis current feedback
ω_{re}	Virtual rotor speed reference
$dq \rightarrow \alpha\beta$	Virtual dq to stationary $\alpha\beta$ transformation
v_a, v_b, v_c	Three-phase
θ_{re}	Virtual rotor position angle
i_a, i_b	Phase A current, Phase B current
i_d, i_q	Virtual d-axis current Virtual q-axis current
v_d, v_q	Virtual d-axis voltage reference Virtual q-axis voltage reference
$\frac{1}{s}$	Integrator module
$abc \rightarrow dq$	Stationary abc to virtual dq transformation
PI	Proportional-Integral regulator

3.3 *High-frequency rotating voltage injection method*

In the high-frequency rotating voltage injection method, a rotating high-frequency voltage signal is injected into the stationary reference frame, and rotor position information is demodulated from the negative-sequence component of high-frequency current induced by rotor saliency. The implementation block diagram of this method is depicted in Figure 2 [19], and the definitions of variables in the diagram are listed in Table 2. This approach is characterized by favorable system stability and strong robustness. However, it exhibits high dependence on rotor saliency, and the utilization of multiple filters in signal demodulation results in reduced system bandwidth and degraded dynamic performance.

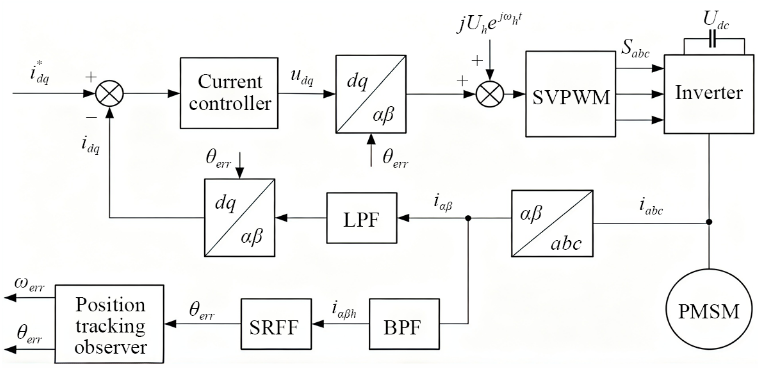

Figure 2. Block diagram of the high-frequency rotating voltage signal injection method

Table 2. Description of symbols in the high-frequency rotating voltage signal injection method

Symbol	Description
i_{dq}^{*}	dq-axis current reference
LPF	Low-Pass Filter
BPF	Band-Pass Filter
SRFF	Synchronous Reference Frame Filter
u_{dq}	dq-axis voltage reference
S_{abc}	Three-phase switching signals
θ_{err}	Estimated rotor position (or position error)
ω_{err}	Estimated rotor speed
$jU_h e^{j\omega_h t}$	High-frequency rotating voltage signal
$abc \rightarrow \alpha\beta$	Coordinate transformation from three-phase stationary abc frame to stationary $\alpha\beta$ frame

The high-frequency rotating voltage signal injection method consists of injecting two orthogonal high-frequency voltage signals into the two-phase stationary $\alpha\beta$ reference frame. Rotor position information is demodulated from the high-frequency current response caused by rotor saliency. The injected signals can be expressed as:

$$\mathbf{u}_{\alpha\beta i} = \begin{bmatrix} u_{\alpha i} \\ u_{\beta i} \end{bmatrix} = \begin{bmatrix} V_i \cos(\omega_i t) \\ V_i \sin(\omega_i t) \end{bmatrix}. \tag{4}$$

Where $\mathbf{u}_{\alpha\beta i}$ is the high-frequency injected voltage vector in the two-phase stationary $\alpha\beta$ coordinate system, $u_{\alpha i}$ is the high-frequency voltage component on the α-axis, $u_{\beta i}$ is the high-frequency voltage component on the β-axis, V_i is the amplitude of the i-th high-frequency injected voltage, ω_i is the angular frequency of the high-frequency injection signal, and t is the time variable.

High-frequency signals are directly injected into the stationary reference frame in this method, with no need for prior estimation of the rotor position, thus yielding favorable stability. Nevertheless, the method relies strongly on motor rotor saliency. Furthermore, the use of multiple filters in signal demodulation reduces system bandwidth and dynamic performance, while phase delay tends to impair estimation accuracy [20].To overcome these drawbacks, an online compensation approach using positive-sequence current components is proposed in Reference [20], which enhances rotor position estimation accuracy. An estimation method based on self-injected harmonic signals is presented in Reference [21], which avoids additional high-frequency signal injection and eliminates the degradation of estimation accuracy caused by low-pass filters. A multi-frequency injection strategy is adopted in Reference [22], where the amplitudes of three-phase high-frequency currents are computed via discrete Fourier transform to detect the rotor sector, allowing initial position acquisition without parameter tuning.

3.4 *High-frequency pulsating voltage injection method*

In the high-frequency pulsating voltage signal injection method, a high-frequency cosine voltage signal is injected into the d-axis of the estimated synchronous rotating reference frame, as expressed in Equation (5). Current signals containing rotor position error are extracted via band-pass filters and low-pass filters, and the estimated rotor position is obtained after signal processing. The implementation block diagram of this method is illustrated in Figure 3 [23], and the definitions of variables in the diagram are listed in Table 3.

$$\mathbf{u}_{dqi} = \begin{bmatrix} V_i \cos(\omega_i t) \\ 0 \end{bmatrix}. \tag{5}$$

Where $\mathbf{u}_{dqi}$ is the high-frequency injected voltage vector in the synchronous d-q coordinate system, V_i is the amplitude of the high-frequency injection voltage, ω_i is the angular frequency of the high-frequency signal, and t is the time variable.

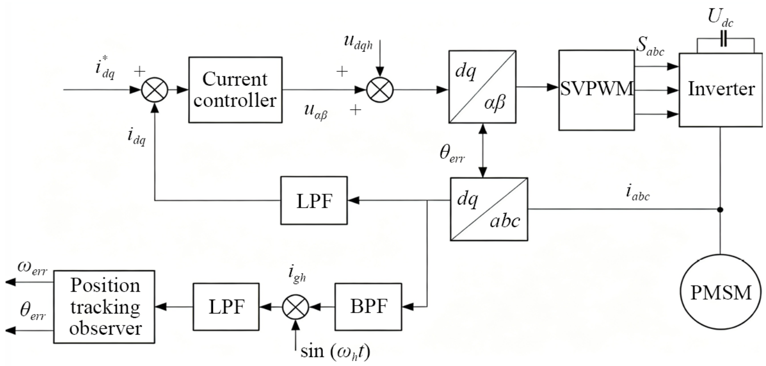

Figure 3. Block diagram of the high-frequency pulsating voltage signal injection method

Table 3. Symbol description for the high-frequency pulsating voltage signal injection method

Symbol	Description
i^*_{dq}	dq-axis current reference
BPF	Band-Pass Filter
LPF	Low-Pass Filter
u_{dq}	dq-axis voltage reference
S_{abc}	Three-phase switching signals
θ_{err}	Estimated rotor position (or position error)
ω_{err}	Estimated rotor speed
u_{dqh}	High - frequency pulsating voltage signal
$abc \rightarrow dq$	Coordinate transformation from stationary abc frame to rotating dq frame
$\sin(\omega_h t)$	High-frequency synchronous demodulation reference signal

Compared with the high-frequency rotating voltage injection method, the high-frequency pulsating voltage injection method shows lower dependence on motor saliency and is applicable to surface-mounted permanent magnet synchronous motors. Nevertheless, this method is still subject to problems including long convergence time and limited system stability induced by filters.

In Reference [24], high-frequency positive-sequence and negative-sequence currents are utilized to improve the signal-to-noise ratio, and the DC offset caused by system delay is eliminated. A direct signal demodulation approach is proposed in Reference [25] to replace synchronous demodulation, and the recursive discrete Fourier transform amplitude normalization technique is adopted to reduce the influences of injected signals and motor parameters. In Reference [26], the second-order generalized integrator is combined with notch filtering to enhance harmonic attenuation capability and broaden the observer bandwidth. Model predictive control is employed in Reference [27] to substitute the PI control in the speed loop, thus alleviating the phase lag effect caused by filters.

3.5 *High-frequency square-wave voltage injection method*

The high-frequency square-wave voltage injection method represents an improved scheme that has undergone rapid development in recent years. A high-frequency square-wave voltage signal is injected into the d-axis of the estimated synchronous rotating reference frame, and the injection frequency can be increased up to the inverter switching frequency.

Since the injection frequency is considerably higher than the cutoff frequency of the current loop, low-pass filters can be eliminated, thereby improving the dynamic performance and bandwidth of the system while reducing audible noise [28].

In Reference [29], a periodic positive-negative injection strategy is adopted to estimate the rotor position. Subtraction is performed between the current integration terms obtained from positive and negative injections, which minimizes dead-time voltage errors without additional compensation. Experimental results indicate that the proposed method yields small fluctuations in position estimation error and achieves a high current-loop bandwidth. The primary challenge of the square-wave injection method lies in its high sensitivity to non-ideal inverter characteristics, such as dead-time effects and device voltage drops, which must be suppressed through symmetric injection or compensation strategies.

A comparison of the above five sensorless control methods under zero and low-speed conditions is presented in Table 4.

Table 4. Sensorless control methods under zero and low-speed conditions

Control method	Advantages	Dynamic response	Core loss type
V/F control	Independent of motor parameters; simple control implementation; low cost	Slow	Copper loss, iron loss
I/F control	Closed-loop current regulation; no inrush current at startup; controllable output torque	Medium	Copper loss, switching loss
High-frequency rotating voltage injection method	Good system stability; strong robustness	Fast	Switching loss, high-frequency iron loss
High-frequency pulsating voltage injection method	Applicable to surface-mounted permanent magnet synchronous motors; relatively simple structure	Fast	High-frequency copper loss, harmonic loss
High-frequency square-wave voltage injection method	Fast dynamic response; reduced filter delay; less dependent on motor parameters	Medium	Copper loss, low-frequency iron loss

4. Model-based observer methods for medium- and high-speed operations

4.1 *Model Reference Adaptive Control (MRAC)*

MRAC is one of the most widely employed approaches for sensorless control of Permanent Magnet Synchronous Motors (PMSMs). MRAC is composed of three core modules: a reference model, an adjustable model, and an adaptation law. The underlying principle is to designate the motor with fixed parameters as the reference model and the fundamental mathematical model of the motor as the adjustable model. The deviation between the adjustable model and the reference model is adjusted by means of a suitable adaptation law, thereby enabling extraction of the rotor position and rotational speed information of the motor [30]. The block diagram for rotor position estimation is depicted in Figure 4, and the definitions of variables in the diagram are listed in Table 5.

However, Model Reference Adaptive System (MRAS) presents distinct limitations in Flywheel Energy Storage (FES) applications. First, high precision of motor parameters is required. Temperature rise during prolonged high-speed operation of FES motors, together with magnetic saturation and cross-coupling effects induced by high charge-discharge currents, gives rise to drifts in stator resistance and d/q-axis inductance [31]. Secondly, the Model Reference Adaptive System (MRAS) suffers from unsatisfactory low-speed performance. Parameter drift will lead to model mismatch and significantly degrade estimation accuracy [32]. In the low-speed region during motor startup and braking, the back Electromotive Force (back EMF) has small amplitude and low Signal-to-Noise Ratio (SNR), which easily results in large estimation errors and deteriorates the start-stop stability of the system. To tackle the aforementioned problems, improved investigations have been carried out from three perspectives: online identification of motor parameters, optimal design of adaptation laws, and low-speed performance improvement. The details are elaborated as follows.

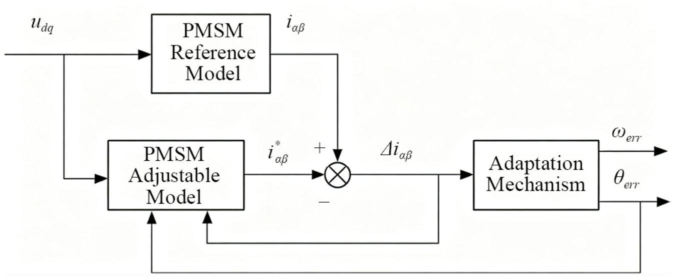

Figure 4. Block diagram of rotor position estimation based on MRAS

Table 5. Symbol description for the MRAS-based rotor position estimation

Symbol	Description
u_{dq}	Stator voltage vector in the synchronous rotating d-q coordinate system
$i_{\alpha\beta}$	Actual stator current vector in the two-phase stationary $\alpha\beta$ coordinate system
$i^*_{\alpha\beta}$	Estimated stator current vector in the two-phase stationary $\alpha\beta$ coordinate system
$\triangle i_{\alpha\beta}$	Current error signal between the actual and estimated currents
ω_{err}	Speed estimation error
θ_{err}	Rotor position estimation error

4.1.1 *Online identification of motor parameters for suppression of model mismatch*

Parameter drift induced by temperature rise and magnetic saturation constitutes the primary cause of model mismatch in MRAS, which directly impairs the speed regulation accuracy and charge-discharge efficiency of flywheel energy storage systems. The integration of online parameter identification with MRAS represents a key strategy for enhancing the robustness of MRAS in flywheel energy storage applications. By identifying drifting parameters in real time and updating them into the adjustable model, dynamic correction of the motor model can be realized [33].

Reference [34] added an online stator resistance identification module to MRAS, which can correct resistance parameters in real time. This solves the problem of inaccurate low-speed estimation caused by temperature rise and improves the control stability during motor start-stop stages. By comparing various identification algorithms, MRAS exhibits the best performance in online parameter correction of flywheel energy storage motors due to its excellent dynamic tracking performance and high identification accuracy, which can fundamentally solve the problem of model mismatch [34].

4.1.2 *Optimal design of adaptation laws for enhancement of dynamic response performance*

The adaptation law directly determines the error convergence speed, dynamic response, and steady-state stability of MRAS. Conventional PI-type adaptation laws with fixed parameters tend to exhibit response lag and slow error convergence under sudden load variation conditions during flywheel energy storage charge-discharge switching. Although the first-order sliding mode adaptation law features strong disturbance rejection, it suffers from chattering phenomena, which can induce motor torque ripple and impair system stability.

In Reference [35], the conventional PI adaptation law is upgraded to a sliding mode adaptation law, and a second-order sliding mode adaptation law is further proposed. While retaining strong robustness, the proposed method effectively suppresses chattering. Specifically, the motor speed overshoot is reduced by 1.4%, the convergence time is shortened by 0.5 s, and the steady-state speed error is optimized by 0.04%, which mitigates speed fluctuation during charge-discharge switching.

Reference [36] presents a novel adaptation law based on the Nonlinear Super-Twisting Algorithm (NSTA). The fal function with filtering factors is introduced to accelerate error convergence. Meanwhile, an improved sliding mode adaptation law with a fast exponential reaching law is designed, and system state variables are adopted to further increase the convergence rate. In addition, the hyperbolic tangent function replaces the sign function to eliminate chattering. This scheme not only satisfies the rapid response requirement of high-speed charge and discharge for flywheel energy storage, but also enhances the operational stability of the motor.

The optimization of adaptation laws realizes the coordinated improvement of error convergence, dynamic response and steady-state stability, and addresses the drawbacks of slow response and severe torque ripple existing in traditional strategies under sudden load variations.

4.1.3 *Low-speed performance optimization and start-stop stability improvement*

In the low-speed range during the start and stop process of flywheel energy storage motors, the back electromotive force has a low amplitude and a low signal-to-noise ratio. The conventional back-EMF observation-based MRAS suffers from large estimation errors, which easily causes dynamic response lag and even motor out-of-step, thereby deteriorating the start-stop stability of the system. To satisfy the wide speed range operation demands of flywheel energy storage, relevant studies optimize low-speed performance from multiple aspects, including observation model improvement, segmented control and hybrid control integration.

To address the poor low-speed performance of the conventional back-EMF model, the stator current model or stator flux model is adopted to replace to optimize the structure of the MRAS observation model. This method effectively improves the speed estimation accuracy in the low-speed region and strengthens the control stability during motor startup. In addition, a hybrid observer combining the high-frequency pulsating voltage injection method with MRAS is designed in Reference [37]. The pulsating high-frequency voltage injection is applied in the low-speed region, while MRAS is adopted for medium and high-speed operation. Meanwhile, a smooth switching strategy is formulated for the transition interval, realizing full-speed-range sensorless control. The hybrid scheme enables MRAS to adapt to the full-speed operation of flywheel energy storage motors and further enhances the start-stop stability of the system.

4.2 *Sliding mode observer method*

As a type of observer-based estimation method, the sliding mode observer transforms the control loop in the state observer into a sliding mode variable structure. It estimates the back EMF using the measurable voltage and current in the PMSM control system, and designs the sliding mode surface based on this relationship. The block diagram of rotor position estimation based on the Sliding Mode Observer (SMO) is shown in Figure 5 [38], and the definitions of variables in the diagram are listed in Table 6.

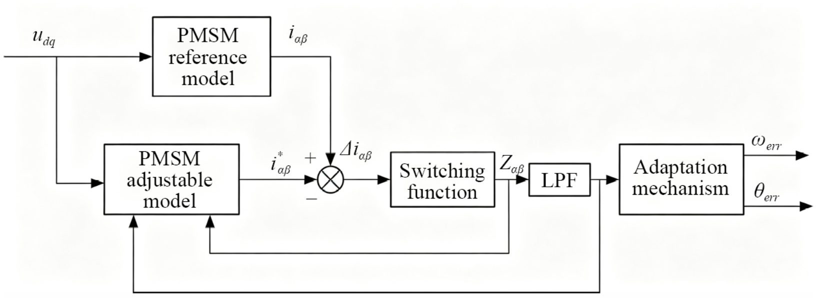

Figure 5. Block diagram of rotor position estimation based on SMO

The back EMF contains the information of rotor position and speed, which enables the indirect estimation of rotor position and speed. When the system operates in sliding mode motion, its performance is entirely determined by the sliding mode surface. Therefore, SMO has the advantages of insensitivity to motor parameter variations and strong robustness.

The conventional SMO usually adopts the sign function as the switching function, resulting in inherent chattering in the SMO. To suppress the abundant switching signals in the back EMF, low-pass filters are commonly introduced. However, the application of low-pass filters causes phase lag, thereby reducing the accuracy of rotor position identification. Accordingly, the research on improved SMO strategies mainly focuses on two aspects: the selection of switching functions and phase compensation.

Table 6. Symbol description for the SMO-based rotor position estimation

Symbol	Description
u_{dq}	Stator voltage vector in the synchronous rotating d-q coordinate system
$i_{\alpha\beta}$	Measured stator current vector in the two-phase stationary $\alpha\beta$ coordinate system
$i^{*}_{\alpha\beta}$	Estimated stator current vector in the two-phase stationary $\alpha\beta$ coordinate system
$\triangle i_{\alpha\beta}$	Current error signal
$Z_{\alpha\beta}$	Processed error signal output by the switching function
ω_{err}	Speed estimation error
θ_{err}	Rotor position estimation error

4.2.1 *Chattering suppression and smooth control*

The discontinuity of switching functions is the fundamental cause of chattering in sliding mode observers. Hence, optimizing the switching function and realizing the smooth transition of sliding mode motion is the core research direction for chattering suppression. At present, the mainstream improvement scheme is to replace the traditional sign function with continuous and smooth functions, which can eliminate high-frequency chattering while ensuring system robustness.

To address the chattering problem of flywheel energy storage motors during medium- and high-speed operation, the hyperbolic tangent function is adopted in Reference [39] to replace the traditional sign function. Relying on the continuous and smooth characteristics of the hyperbolic tangent function, a gradual transition in the switching process is realized, which effectively suppresses chattering. This method not only reduces the design complexity of filtering and phase compensation links, but also improves the estimation accuracy of rotor position and speed, and greatly decreases the position estimation error of flywheel motors under medium and high-speed conditions.

To further optimize the chattering suppression effect, a piecewise exponential function is proposed as the switching function in Reference [40]. This function presents continuous exponential variation characteristics inside the boundary layer and maintains saturation characteristics outside the boundary layer, which ensures the rapid convergence of the system and weakens chattering to the greatest extent. In addition, switching strategies based on continuous functions such as the sigmoid function and improved saturation function have been widely investigated. By introducing boundary layer parameters or shape adjustment coefficients, these functions can achieve a flexible trade-off between robustness and chattering suppression, adapting to diverse operating conditions of flywheel energy storage systems [41].

Since the traditional fixed-gain switching function cannot balance system convergence speed and chattering suppression, an adaptive sliding mode gain strategy is adopted to dynamically adjust the sliding mode gain according to the speed variation and current observation error of flywheel motors [42]. For instance, a smaller gain is applied in the low-speed region to reduce chattering, while the gain is increased under medium-high speed or sudden load changes to guarantee rapid system convergence. This strategy significantly improves the comprehensive performance of sliding mode observers in a wide speed range.

In Reference [43], an adaptive reaching law is combined with a continuous switching function to design a novel exponential adaptive sliding mode observer. The adaptive law is used to process high-order harmonic components in the equivalent back-EMF signal, which avoids the application of low-pass filters and further simplifies the system structure.

4.2.2 *Filtering and phase compensation*

Although the adoption of low-pass filters can suppress chattering to a certain extent, it inevitably leads to phase lag of back-EMF signals and further causes deviation in rotor position estimation. Such adverse effects are particularly prominent when flywheel motors operate at high speed, which greatly deteriorates the system control performance. Therefore, the optimization of filtering schemes and phase compensation strategies has become a key measure to improve the estimation accuracy of sliding mode observers.

To address the position estimation deviation of sliding mode observers for high-speed flywheel motors, an adaptive low-pass filter phase compensation method is proposed in Reference [44]. An improved integral terminal sliding mode controller is designed with a fast sliding surface and continuous reaching law, which eliminates chattering caused by conventional discontinuous switching functions and guarantees the finite-time convergence of system states. Furthermore, an Extended State Observer (ESO) is introduced to to estimate real-time internal uncertainties and external disturbances. The disturbances are offset via feedforward compensation, thereby enhancing the adaptability of the control system to complex operating conditions.

To avoid the phase delay induced by traditional low-pass filters, Adaptive Synchronous Filters (ASF) are adopted to replace low-pass filters in References [45], [46]. The amplitude-frequency characteristics of ASF can be dynamically adjusted with motor speed. They can not only effectively suppress high-frequency noise and harmonics, but also eliminate phase lag. Especially in the low-speed region with a low signal-to-noise ratio, the combination with a back-EMF estimator can further improve the estimation accuracy.

In addition, a Position Error Cancellation Phase-Locked Loop (PECPLL) strategy is proposed in Reference [47]. By cascading a low-pass filter with identical filtering characteristics to those of the sliding mode observer in the feedback loop of the traditional phase-locked loop, the phase delay generated by the filtering link is automatically eliminated, achieving accurate estimation of rotor position signals. This method is not affected by the accuracy of the estimated speed and can better filter high-frequency sliding mode noise, which significantly improves the estimation accuracy of position and speed for flywheel motors during medium- and high-speed operation.

4.3 *Extended Kalman filter method*

The Extended Kalman Filter (EKF) is an optimal state estimation algorithm for systems with process noise and measurement noise. With known noise covariance matrices, EKF can achieve optimal noise filtering. Furthermore, it enables accurate estimation of rotor position and speed without requiring the initial rotor position and mechanical parameters. The implementation block diagram of the EKF algorithm is illustrated in Figure 6 [48], and the definitions of variables in the diagram are listed in Table 7.

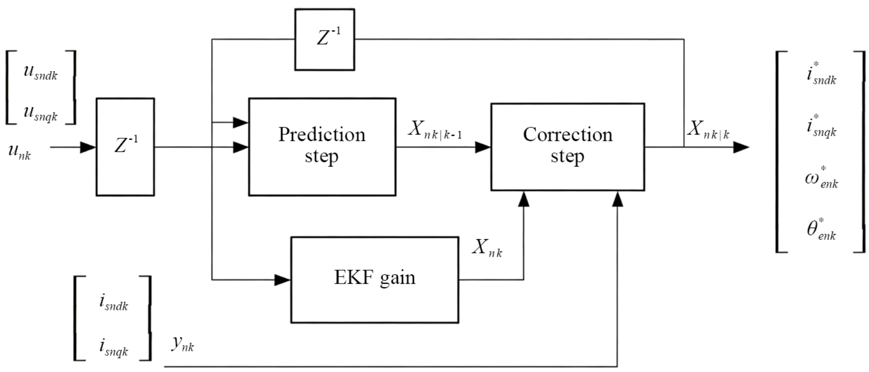

Figure 6. Block diagram of extended Kalman filter algorithm implementation

The major advantages of EKF lie in its excellent suppression capability against system and measurement noise, as well as the independence from initial rotor position information, which facilitates digital engineering implementation. Scholars worldwide have carried out in-depth research on EKF improvement, mainly focusing on covariance matrix optimization and order reduction processing.

Table 7. Block diagram of extended Kalman filter algorithm implementation description

Symbol	Description
$\begin{bmatrix} u_{sndk} \\ u_{snqk} \end{bmatrix}$, $\begin{bmatrix} i_{sndk} \\ i_{snqk} \end{bmatrix}$, $\begin{bmatrix} i^*{}_{sndk} \\ i^*{}_{snqk} \\ \omega^*_{enk} \\ \theta^*_{enk} \end{bmatrix}$	Input voltage vector in the synchronous rotating frame, Measured output vector, Rotor position estimation error
Z^{-1}	Unit delay operator
$X_{nk\|k-1}$	A priori state estimate
EKF gain	Extended Kalman gain matrix
$X_{nk\|k}$	A posteriori state estimate
X_{nk}	Intermediate variable related to the Kalman gain calculation

4.3.1 *Covariance matrix optimization*

In terms of covariance matrix optimization, the statistical characteristics of system noise and measurement noise are usually difficult to acquire accurately. Consequently, the selection of covariance matrices acts as a key factor determining the estimation performance of EKF. To satisfy the demand for real-time adjustment of covariance matrices under variable operating conditions within the wide speed range of flywheel energy storage systems, an adaptive extended Kalman filter algorithm based on the innovation sequence is proposed in Reference [49]. By online regulating the noise covariance matrix, the proposed method improves the EKF estimation accuracy under the interference of gross errors and noise statistical deviation.

Reference [50] develops an enhanced EKF framework capable of simultaneously estimating system states and external disturbances. Disturbance variables are expanded into additional system states. Compared with the traditional stepwise estimation scheme, this approach greatly enhances the estimation accuracy of rotor speed and position under load disturbances, providing a novel technical solution for high-precision sensorless control of flywheel motors under complex disturbance conditions.

4.3.2 *Order reduction processing*

In terms of order reduction, flywheel energy storage systems impose high requirements on algorithm real-time performance. Reducing the computational burden of EKF is critical to improving its engineering practicability. An Adaptive Reduced-order Extended Kalman Filter (AREKF) is proposed in Reference [51]. By selecting partial state variables of the motor model, the order of EKF is reduced, and a scalar Kalman filter is adopted to correct the predicted values of unmodeled states. Analysis based on floating-point operation calculation verifies that this method can reduce the algorithm complexity by nearly 40%.

Aiming at the problem that reduced-order EKF is sensitive to noise in the low-speed region, Reference [52] presents a reduced-order EKF scheme combined with the eight-quadrant Newton-Raphson method. It cuts down the computational cost while maintaining estimation robustness under speed reversal and noise interference.

4.4 *Proportional-Integral-Derivative (PID) control*

PID control is the most fundamental and widely used regulation method in vector control for PMSMs in flywheel energy storage systems. It typically forms a dual closed-loop structure consisting of an outer speed loop and an inner current loop. The block diagram of the PID control structure is shown in Figure 7, and the definitions of variables in the diagram are listed in Table 8. The speed-loop PI controller outputs the torque current command according to the speed error, while the current-loop PI controller achieves fast tracking of the dq-axis currents. Combined with decoupling compensation and Space Vector Pulse Width Modulation (SVPWM) modulation, precise regulation of motor torque and speed is realized [53].

However, flywheel energy storage systems are characterized by a wide speed range, frequent charge-discharge switching, and variations in motor parameters caused by temperature changes and magnetic saturation. Conventional PID controllers with fixed parameters struggle to balance dynamic response speed and steady-state accuracy across the full speed range and all operating conditions, and suffer from inherent drawbacks such as large overshoot, weak anti-load disturbance capability, and poor parameter adaptability. To address these issues, research on improved PID control strategies mainly focuses on three aspects: controller structure optimization, parameter adaptive adjustment, and intelligent algorithm optimization.

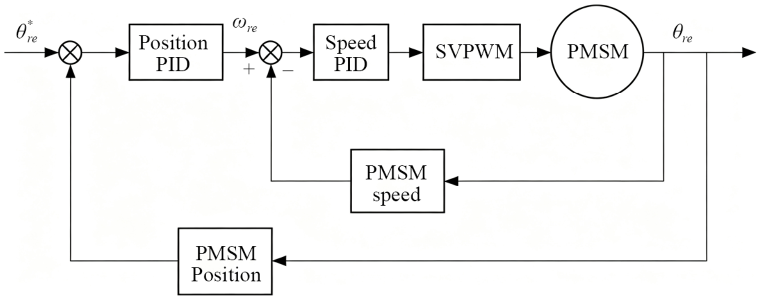

Figure 7. Block diagram of PID control principle

Table 8. Symbol description for the PID control principle

Symbol	Description
θ^*_{re}	Reference rotor position
ω_{err}	Speed reference command
θ_{re}	Actual rotor position
Position PID	Position loop proportional-integral-derivative regulator
Speed PID	Speed loop proportional-integral-derivative regulator

4.4.1 *In terms of controller structure improvement*

Conventional single-loop PID controllers cannot balance rapidity and stability at the same time. In Reference [54], the controller is divided into an outer loop and an inner loop. The outer loop adopts PI control to guarantee zero steady-state error, while the inner loop applies Proportional-Derivative (PD) control with filtering coefficients or a (1 + PD) structure to accelerate dynamic response and suppress high-frequency noise. This control structure is applied to the AGC of interconnected power grids with flywheel energy storage. Benefiting from the cooperative work of inner and outer loops, the settling time is greatly shortened and the overshoot is effectively reduced.

To address the position out-of-step issue of dual PMSM drive systems under independent control, which is vulnerable to load disturbances, a cross-coupled current loop structure is proposed in Reference [55]. By mutually introducing the state variables of the two motors into their respective controllers, collaborative regulation is realized. This method remarkably improves synchronization accuracy and anti-load disturbance capability of the system.

4.4.2 *Parameter self-tuning and adaptive adjustment*

To address the limitation that fixed PID parameters fail to adapt to time-varying operating conditions, a fuzzy self-tuning mechanism is introduced in Reference [56]. With the system error and its change rate as input variables, PID gains are adjusted online based on fuzzy rules. In thermal power-flywheel combined frequency regulation and metro regenerative braking energy storage systems, fuzzy PID control presents superior dynamic response and steady-state accuracy compared with conventional PID. Further combining particle swarm optimization to optimize fuzzy rules or scaling factors can effectively improve the adaptability of the controller.

For inertial flywheel systems, sudden variations in power commands tend to trigger severe power fluctuations under fixed PID parameters. In Reference [57], model-free reinforcement learning is utilized to train a neural network agent, which takes power deviation, motor speed and other state variables as inputs and outputs three PID parameters in real time. This strategy does not rely on an accurate system model and can adapt online to complex working conditions. It greatly reduces power overshoot and fluctuation, and achieves better dynamic performance than traditional fixed-parameter PID control.

4.4.3 *Integration of intelligent algorithms and PID*

In finite-set model predictive speed control, conventional methods are plagued by steady-state errors and torque ripple. In Reference [58], a proportional-integral-differential cost function is designed, where the integral term eliminates steady-state errors and the differential term suppresses torque ripple. Meanwhile, the prediction-correction method is adopted for speed measurement, and a Kalman filter is combined to observe load torque. Compared with traditional schemes, the improved control strategy significantly reduces the total harmonic distortion of current and achieves a faster dynamic response. In addition, aiming at the application of flywheel energy storage in metro regenerative braking, the particle swarm optimized fuzzy PID proposed in Reference [59] is superior to traditional PI and conventional fuzzy PID in terms of response speed, overshoot and steady-state accuracy.

Table 9. Performance comparison of four main model-based sensorless control algorithms

Algorithm type	Anti-disturbance ability	Parameter sensitivity	Computational complexity	Application scenario	Dominant energy loss type
MRAC	Moderate	High	Low	Medium-low speed and stable operating conditions	Copper loss, switching loss
SMO	Strong	Moderate	Medium	High-speed and strong interference conditions	Switching loss, high-frequency iron loss
EKF	Strong	Low	High	High-precision and complex operating conditions	Algorithm calculation power consumption, copper loss
PID	Medium	Medium	Low	Most feedback control applications	Copper loss, fundamental iron loss

A comparison of the advantages and disadvantages of the above four model-based observer methods for medium- and high-speed operations is presented in Table 9.

5. Full-speed-range operating condition control method

Traditional methods can hardly achieve stable operation of flywheel energy storage PMSMs from standstill to ultra-high speed. To solve this problem, this paper proposes a full-speed-range sensorless control strategy suitable for flywheel energy storage PMSMs. The high-frequency voltage injection method is adopted to realize accurate rotor position observation in the low-speed region, and an improved sliding mode observer is used to suppress chattering and improve estimation accuracy in the medium-high speed region. A weighted smooth switching algorithm is designed to achieve seamless connection between the two observers.

The estimated motor speed is taken as the switching criterion, and the switching threshold range is set as follows:

When the speed is lower than 400 rpm, the output of high-frequency injection is dominant; when the speed is higher than 800 rpm, the output of the sliding mode observer is dominant; the range of 400 ~ 800 rpm is defined as the transition zone, in which the outputs of the two observers are fused by linear weighting to realize impact-free transition.

To verify the effectiveness of the proposed hybrid control strategy, a full-speed-range sensorless control simulation model for the flywheel energy storage PMSM is established, with emphasis on analyzing the tracking performance of rotor position and speed. The simulation conditions are set as follows: the motor operates in the high-frequency injection control zone and realizes sensorless starting from 0 to 0.4 s; it runs stably from 0.5 s to 1 s to provide sufficient convergence time for the SMO and avoid switching shocks; it enters the SMO closed-loop control zone and completes medium-high speed acceleration from 1 s to 2 s; and it maintains steady-state operation at rated speed after 2 s. The analysis of simulation results is given below:

The speed tracking curve is shown in Figure 8. During the acceleration phase, only a small dynamic error exists between the actual speed and the estimated speed at the initial start-up stage, with no obvious lag or overshoot. During steady-state operation, the actual speed and estimated speed almost completely coincide, and the steady-state error is controlled within ±2%. The curve only has tiny high-frequency ripples, which conform to the normal characteristics of the sliding mode observer. This indicates that the SMO in the medium-high speed region can achieve high-precision speed estimation with good robustness.

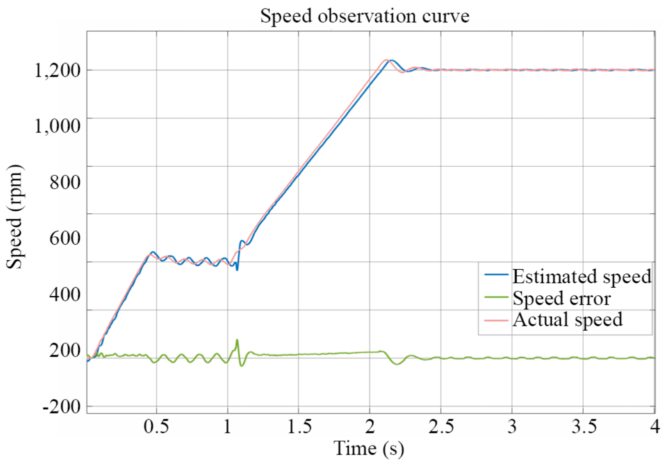

Figure 8. Speed tracking curve

The rotor position tracking curve is shown in Figure 9. In the low-speed starting stage, the estimated position can quickly follow the actual position without phase deviation or divergence, which verifies the position demodulation capability of the high-frequency injection method at zero and low speeds and ensures the position synchronization of the starting process. In the medium-high speed steady-state operation stage, the actual and estimated position curves are completely synchronized, and the position error is always controlled within ± 0.05 rad without phase deviation or error accumulation, which verifies the position estimation accuracy of the dual observers and the effectiveness of the smooth switching strategy.

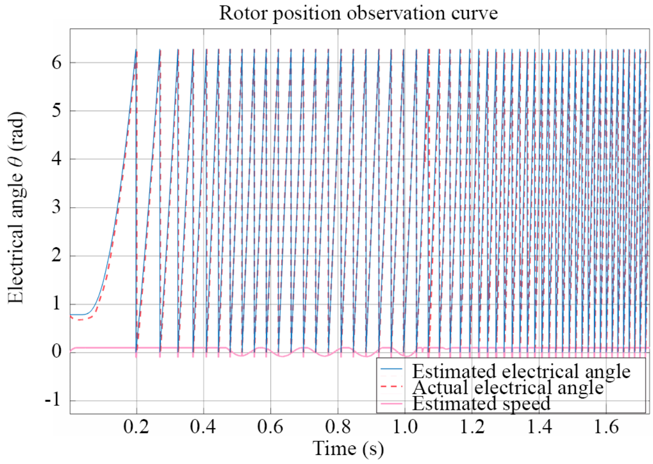

Figure 9. Rotor position tracking curve

The simulation results demonstrate that the proposed hybrid control scheme can achieve sensorless closed-loop control of the flywheel energy storage motor from zero speed to medium-high speed. There is no out-of-step in the low-speed region, high precision in the medium-high speed region, and no impact during the switching process. The speed and position tracking performance meets the requirements of design specifications, which is suitable for the wide-speed-range and high-stability operation characteristics of flywheel energy storage systems.

6. Outlook

The core of sensorless control for flywheel energy storage motors lies in the accurate detection and estimation of the motor rotor position. Each method has its own limitations; therefore, multi-algorithm fusion and advantage complementarity have become the mainstream technical route. However, how to achieve smooth switching and cope with parameter drift and disturbances in the wide speed range is the key challenge of hybrid control.

Long-term high-speed operation, temperature rise and magnetic saturation cause variations in motor parameters, leading to model mismatch and position estimation errors. Open-loop V/F and I/F strategies may lose synchronization under severe load fluctuations. In addition, high-frequency injection methods accelerate power device aging and induce parameter drift of passive filter components.

Grid voltage fluctuations and sudden load disturbances affect observer convergence and cause transient oscillations during algorithm switching. High-frequency excitation produces electromagnetic noise and torque ripple, which deteriorates long-term operating stability. Moreover, single observation algorithms lack redundant fault-tolerant logic, weakening system reliability under abnormal conditions.

The future development trends of sensorless control for flywheel energy storage mainly include the following three aspects:

(1) Aiming at the problems of ultra-high speed operation and time-varying parameters, it is necessary to develop new observation theories and compensation methods. Research should be conducted on discrete-domain reduced-order observation and deadbeat predictive compensation to improve high-speed estimation accuracy under low carrier ratio. In addition, online identification of multiple parameters such as d/q-axis inductance and stator resistance into the observation model to compensate for model mismatch caused by temperature rise and magnetic saturation, thereby enhancing the robustness of the system during long-term operation.

(2) It is essential to improve the switching stability and anti-disturbance capability of hybrid control strategies. A full-speed-range hybrid observation structure combining high-frequency signal injection, the sliding mode observer, and model reference adaptive control should be constructed, and impact-free operation from standstill to ultra-high speed

should be realized through smooth switching strategies. At the same time, based on strong anti-disturbance theories such as super-twisting sliding mode and the extended state observer, disturbances caused by sudden load changes and inverter nonlinearity should be suppressed to ensure reliable switching in the transition interval.

(3) Intelligent autonomous control should be achieved with the help of artificial intelligence. Intelligent optimization algorithms and reinforcement learning should be combined to realize online self-tuning of observer gains and control parameters, thereby eliminating the dependence on accurate motor models. At the same time, for power grid frequency regulation and hybrid energy storage systems, research on flywheel-battery cooperative sensorless control should be carried out to achieve rapid power distribution and frequency stability support, promoting the transformation of sensorless control from theoretical research to system-level engineering applications.

7. Conclusion

At present, there is no single method for the sensorless control of flywheel energy storage motors that can simultaneously meet the control requirements of full-speed range coverage, high precision, and strong robustness. Multi-algorithm fusion has become the mainstream development direction. From the perspective of engineering practice, existing technologies still generally have shortcomings such as high algorithm complexity and insufficient model adaptability, and there is still a certain gap from large-scale engineering application.

In the future, the development of sensorless control for flywheel energy storage should be guided by engineering needs. While continuously optimizing observation algorithms and improving control performance, we should focus on the lightweight and practical transformation of technologies, and strive to reduce the cost of hardware implementation and debugging. By breaking through key technical bottlenecks such as ultra-high-speed modeling, smooth switching, and multi-unit coordination, and promoting the in-depth integration of artificial intelligence and traditional control technologies, one is expected to achieve the leap of sensorless control from laboratory verification to mass production engineering. This will provide core technical support for the wide application of flywheel energy storage in fields such as power grid energy storage and new energy power generation, thereby fully exerting its technical advantages of high efficiency, flexibility, and long service life.

Author contributions

Conceptualization, S.Y., J.W. (Junying Wei), J.W. (Jihong Wang) and S.L. and Y.Y. ; methodology, S.Y.; software, S.Y.; validation, S.Y.; investigation, S.Y.; resources, J.W. (Junying Wei) and J.W. (Jihong Wang); data curation, S.Y.; writing-original draft preparation, S.Y.; writing-review and editing,Y.Y. J.W. (Junying Wei) and J.W. (Jihong Wang); visualization, S.Y.; supervision, J.W. (Junying Wei) and J.W. (Jihong Wang); project administration, J.W. (Junying Wei) and J.W. (Jihong Wang); funding acquisition, J.W. (Junying Wei) and J.W. (Jihong Wang).All authors have read and agreed to the published version of the manuscript.

Funding

This research was funded by Cooperative Research on Composite Energy Storage Technology of Flywheel and Compressed Air Energy Storage, grant number 2024YFE0208100.

Data availability statement

The raw simulation data generated in this study are available from the author upon reasonable request.

Acknowledgements

The authors express their thanks to the people helping with this work. In the preparation of this work, the authors used Gemini to assist with text editing and formatting refinement. After using this tool/service, the authors reviewed and edited the content as needed, and take full responsibility for the content of the publication.

Conflict of interest

The authors declare no conflicts of interest.

References

[1] R. Takarli, A. Amini, M. Khajueezadeh, M. S. Zarbil, A. Vahedi, A. Kiyoumarsi, H. Tarzamni, and J. Kyyra, "A comprehensive review on flywheel energy storage systems: survey on electrical machines, power electronics converters, and control systems," *IEEE Access*, vol. 11, pp. 81224-81255, 2023.

[2] W. Ji, F. Hong, Y. Zhao, L. Liang, H. Du, J. Hao, F. Fang, and J. Liu, "Applications of flywheel energy storage system on load frequency regulation combined with various power generations: A review," *Renewable Energy*, vol. 223, p. 119975, 2024.

[3] K. Xu, Y. Guo, G. Lei, and J. Zhu, "Sensorless control of high-speed PMSM based on cascade high-order extended state observer for flywheel energy storage system," *IEEE Transactions on Industrial Electronics*, vol. 73, no. 2, pp. 1738-1749, 2026.

[4] Q. Wang, H. Yuan, X. Jiang, and X. Xing, "A simple sensorless control strategy for IPMSM in 1 MW flywheel energy storage system," in Proc. IEEE International Power Electronics and Motion Control Conference, 2016, pp. 1923-1928.

[5] Y. Li, H. Hu, and P. Shi, "A review of position sensorless compound control for PMSM drives," *World Electric Vehicle Journal*, vol. 14, no. 2, p. 34, 2023.

[6] G. Song, Z. Wu, Q. Yan, J. Zhang, P. Yang, and Z. Zhang, "Sensorless fault-tolerant control strategy of flywheel energy storage system based on improved model reference adaptive system," *Journal of Energy Storage*, vol. 132, p. 117842, 2025.

[7] F. Xu, X. Dai, Y. Wang, D. Hu, H. Zhang, and H. Chen, "Research progress on permanent magnet machines for flywheel energy storage," *Energy Storage Science and Technology*, vol. 13, no. 10, pp. 3423-3441, 2024.

[8] J. X. Xing and X. Jiang, "Introduction to motors and controllers of flywheel energy storage systems," *Energy Storage Science and Technology*, vol. 4, no. 2, pp. 147-152, 2015.

[9] X. Zhu, K. Huang, and S. Huang, "A stable V/F control method of high-speed permanent magnet synchronous motor," *Power Electronics*, vol. 52, no. 7, pp. 28-32, 2018.

[10] A. Cheng and X. Jin, "A stable V/F control method for permanent magnet synchronous motor drives," in Proc. IEEE Transportation Electrification Conference and Expo, Asia-Pacific, 2017, pp. 1-5.

[11] Y. Zhang, Z. Yin, J. Liu, R. Zhang, and X. Sun, "IPMSM sensorless control using high-frequency voltage injection method with random switching frequency for audible noise improvement," *IEEE Transactions on Industrial Electronics*, vol. 67, no. 7, pp. 6019-6030, 2020.

[12] L. Yu, S. Zhou, F. Cao, Q. Li, and S. Zhang, "A comparative study of position sensorless low speed start methods in surface mounted permanent magnet synchronous motor," *Micromotors*, vol. 57, no. 4, pp. 33-39, 2024.

[13] H. Zhao, W. Zhang, and C. Yang, "A kind of V/f control method for the permanent magnet synchronous motors with a speed feedback loop," *Drive & Control*, no. 6, pp. 10-13, 2024.

[14] Q. Tang, D. Chen, and X. He, "Integration of Improved Flux Linkage Observer and I-f Starting Method for Wide-Speed-Range Sensorless SPMSM Drives," *IEEE Transactions on Power Electronics*, vol. 35, no. 8, pp. 8374-8383, 2020.

[15] Q. Wang, S. H. S. Wang, and C. H. Chen, "Review of sensorless control techniques for PMSM drives," *IEEJ Transactions on Electrical and Electronic Engineering*, vol. 14, no. 10, pp. 1543-1552, 2019.

[16] Y. Zhao, B. Ning, S. Lu, and J. Liu, "Full speed sensorless control method of permanent magnet synchronous motor based on I/F starting and extended Kalman filter," *Electric Machines & Control Application*, vol. 49, no. 2, pp. 1-7, 2022.

[17] S. V. Nair, K. Hatua, N. V. P. R. D. Prasad, and D. K. Reddy, "A quick I-f starting of PMSM drive with pole slipping prevention and reduced speed oscillations," *IEEE Transactions on Industrial Electronics*, vol. 68, no. 8, pp. 6650-6661, 2021.

[18] D. Chen, K. Lu, and D. Wang, "An If startup method for back-EMF based sensorless FOC of PMSMs with improved stability during the transition," in Proc. International Symposium on Industrial Electronics and Applications, 2020, pp. 1-6.

[19] G. Zhang and J. Du, "Review of position sensorless control technology for permanent magnet synchronous motors," *Electric Machines and Control Application*, vol. 51, no. 1, pp. 1-13, 2024.

[20] W. Peng, M. Qiao, C. Jiang, Z. Zhang, and J. Gao, "An online position error compensation method of rotating high-frequency voltage injection based on positive sequence components," *Transactions of China Electrotechnical Society*, vol. 35, no. 24, pp. 5087-5095, 2020.

[21] J. Wei, J. Wang, L. Zhang, Y. Shen, Z. Zhang, and B. Zhou, "Initial rotor position estimation method for aircraft three-stage starter/generator based on self-injected harmonic signal," *IEEE Transactions on Transportation Electrification*, vol. 9, no. 1, pp. 856-865, 2023.

[22] B. Shuang and Z. Q. Zhu, "A novel sensorless initial position estimation and startup method," *IEEE Transactions on Industrial Electronics*, vol. 68, no. 4, pp. 2964-2975, 2021.

[23] Y. Wang, K. Xing, and C. Zhang, "A rotating sythesis vector based high frequency pulse voltage injection method for the sensorless control of the flux-switching permanent magnet machine," *Proceedings of the CSEE*, vol. 42, no. 19, pp. 7224-7235, 2022.

[24] S. Wang, Z. Li, D. Wu, and J. Zhao, "Sensorless control of SPMSM based on high-frequency positive-and negative-sequence current dual-demodulation," *IEEE Transactions on Industrial Electronics*, vol. 70, no. 5, pp. 4631-4639, 2023.

[25] X. Zhang, H. Li, S. Yang, and M. Ma, "Improved initial rotor position estimation for PMSM drives based on HF pulsating voltage signal injection," *IEEE Transactions on Industrial Electronics*, vol. 65, no. 6, pp. 4702-4713, 2018.

[26] D. Kong, W. Li, J. Han, C. Deng, M. Yan, and L. Zhou, "Sensorless control of permanent magnet synchronous linear motor based on improved second-order generalized integrators," in Proc. 5th Asia Conference on Energy and Electrical Engineering, 2022, pp. 90-96.

[27] W. Liu and H. Liu, "Improved sensorless control for pulsating high frequency signal injection of permanent magnet synchronous motor," *Electrical Engineering*, vol. 24, no. 6, pp. 6-12, 2023.

[28] S. Dong, M. Zhou, C. Wang, L. Gou, and X. You, "Improved hybrid sensorless control for IPMSM in full speed range at low switching frequency," *IEEE Transactions on Energy Conversion*, vol. 40, no. 1, pp. 123-135, 2024.

[29] R. Ni, D. Xu, F. Blaabjerg, K. Lu, G. Wang, and G. Zhang, "Square-wave voltage injection algorithm for PMSM position sensorless control with high robustness to voltage errors," *IEEE Transactions on Power Electronics*, vol. 32, no. 7, pp. 5425-5437, 2017.

[30] H. Wang, "Research on speed-sensorless control technology of PMSM based on improved MRAS," M.S. thesis, Harbin University of Science and Technology, Harbin, China, 2022.

[31] N. Jiang, R. Cao, W. Sun, D. Chen, and K. Wang, "MRAS-based sensorless control of PMSM drives using extended state observer in shaftless rim-driven thruster system," *IEEE Transactions on Transportation Electrification*, vol. 11, no. 2, pp. 6038-6047, 2025.

[32] M. Qin and Y. Li, "Sensor less control of permanent magnet synchronous motor with online parameter adaptive function," *Diangong Jishu*, no. 1, pp. 1-11, 2023.

[33] Z. Yun, W. Shan, and G. Bai, "Sensorless control strategy for permanent magnet synchronous spindle in full speed domain," *Modular Machine Tool & Automatic Manufacturing Technique*, no. 1, pp. 1-11, 2023.

[34] C. Weng, “Sensorless control of high power permanent magnet synchronous motor based on model reference adaptive system,” M.S. thesis, Beijing Jiaotong University, Beijing, China, 2022.
[35] D. Liu, X. Dong, F. Wang, J. Zhao, and L. Chen, “Sensorless control under parameter identification of permanent magnet synchronous motor for electric aircraft,” *International Journal of Circuit Theory and Applications*, vol. 54, no. 3, pp. 1696-1713, 2026.
[36] X. Chen, “Research on sensorless control of permanent magnet synchronous motors based on model reference adaptive system,” M.S. thesis, Harbin University of Science and Technology, Harbin, China, 2025.
[37] J. Niu, Y. Yang, J. Xi, and K. Zhang, “Research on sensorless control of permanent magnet synchronous motor at full speed,” *Power Electronics*, vol. 56, no. 4, pp. 48-52, 2022.
[38] Y. Yang and X. Liu, “Position sensorless control of permanent magnet synchronous motors in wide speed range based on improved sliding mode method,” *Electric Machines and Control Application*, vol. 49, no. 7, pp. 7-13, 2022.
[39] Z. Song, J. Zhang, J. Zhao, and W. Guo, “Flywheel energy storage system control method based on the improved sliding mode observer,” *Journal of North China Electric Power University*, vol. 45, no. 5, pp. 36-42, 2018.
[40] M. Li, L. Li, and J. Zhou, “Sensorless vector control of PMSM based on improved sliding mode with variable structure,” *Electric Machines and Control Application*, vol. 51, no. 2, pp. 22-33, 2024.
[41] S. Huang, Y. Huang, L. Wang, and L. Shi, “An adaptive full-order sliding-mode observer based-sensorless control for permanent magnet synchronous propulsion motors drives,” *Vehicles*, vol. 8, no. 2, p. 34, 2026.
[42] S. Chen, X. Chen, X. Hu, H. Wang, Y. Han, and J. Chen, “An improved super-twisting sliding-mode observer for sensorless control of PMSM,” *Journal of System Simulation*, vol. 38, no. 6, pp. 1-7, 2026.
[43] Y. Liu, G. Yang, T. Xu, M. Cheng, and Z. Huang, “Research on sliding mode observer based on hyperbolic tangent function,” *Computer and Digital Engineering*, vol. 50, no. 10, pp. 2312-2317, 2022.
[44] J. Jiang, X. Zhou, W. Zhao, W. Li, and W. Zhang, “A fast integral sliding mode controller with an extended state observer for position control of permanent magnet synchronous motor servo systems,” *Frontiers of Information Technology and Electronic Engineering*, vol. 21, no. 8, pp. 1239-1250, 2020.
[45] W. Liu, L. Zhou, X. Tang, and Z. Qi, “Research on FESS control based on the improved sliding-mode observer,” *Proceedings of the CSEE*, vol. 34, no. 1, pp. 71-78, 2014.
[46] Z. Li, S. Zhou, Y. Xiao, and L. Wang, “Sensorless vector control of permanent magnet synchronous linear motor based on self-adaptive super-twisting sliding mode controller,” *IEEE Access*, vol. 7, pp. 44998-45011, 2019.
[47] X. Sun, D. Wu, R. Wang, S. He, M. Wei, and W. Cui, “Sensorless control of PMSM using adaptive sliding mode observer based on improved PLL,” *Electric Machines and Control Application*, vol. 50, no. 11, pp. 65-73, 2023.
[48] Y. Zhang, Z. Yin, R. Tang, and J. Liu, “Moment of inertia and load torque identification based on adaptive extended Kalman filter for interior permanent magnet synchronous motors,” *IEEE Transactions on Instrumentation and Measurement*, vol. 74, pp. 1-12, 2025.
[49] Y. Sang, Z. Wu, and Y. Fan, “An adaptive extended Kalman filter observer for permanent magnet synchronous motor position sensorless control systems,” *Scientific Reports*, vol. 15, no. 1, p. 11605, 2025.
[50] K. Yu, F. Xiang, J. Su, W. Zhu, and S. Li, “Simultaneous state and disturbances estimation for sensorless PMSM control: Design and experiments,” *IEEE Transactions on Power Electronics*, vol. 40, no. 12, pp. 17750-17760, 2025.
[51] S. Wang and K. Liu, “An adaptive speed estimation method based on a reduce-order extended Kalman filter for PMSM sensorless drives,” in Proc. IEEE 2nd International Conference on Control, Electronics and Computer Technology, 2024, pp. 220-224.
[52] F. Xiang, K. Yu, C. Chen, and S. Li, “Sensorless control of PMSM drives using octant Newton-Raphson method and reduced-order EKF considering speed reversal and noise,” *IEEE Transactions on Power Electronics*, vol. 48, no. 8, pp. 10793-10803, 2025.
[53] Y. Lu, J. Huang, Z. Jiang, T. Tang, H. Tang, and L. Shi, “PID adaptive feedback motor system based on neural network,” *IEEE Access*, vol. 12, pp. 60149-60154, 2024.
[54] Y. Wang, W. Cheng, H. Xue, Y. Zhang, and Y. Mi, “Controller design of an AGC based on a cascade PI-(1 + PD) algorithm for an interconnected power grid with flywheel energy storage,” *Power System Protection and Control*, vol. 51, no. 14, pp. 1-9, 2023.

[55] Y. Wu, X. Xiang, H. Li, W. Li, and S. Chen, “Dual permanent magnet synchronous motor adaptive stability against load disturbance cross-coupling control strategy,” *Proceedings of the CSEE*, vol. 45, no. 1, pp. 319-329, 2025.

[56] D. Kong, J. Liang, B. Qian, and Y. Li, “AGC control strategy for thermal power-flywheel energy storage interconnected power grid considering frequency stability performance,” *Journal of Engineering for Thermal Energy and Power*, vol. 40, no. 12, pp. 119-131, 2025.

[57] R. Sa, C. Wu, Z. Ni, Y. Zhang, X. Jiang, and J. Tian, “A variable-parameter PID active power control strategy of inertial flywheel based on reinforcement learning,” *Energy Storage Science and Technology*, vol. 14, no. 5, pp. 1982-1990, 2025.

[58] J. Qiu, Y. Mao, Z. Chen, and C. Shi, “Improved finite set model predictive speed control of permanent magnet synchronous motor,” *Electric Machines and Control*, vol. 27, no. 4, pp. 1-9, 2023.

[59] W. Zhao, K. Ning, J. Wang, C. Zhang, and W. Ning, “Optimization control method for regenerative braking energy storage in rail transport based on flywheel system,” *Heavy Machinery*, vol. 2026, no. 1, pp. 18-24, 2026.